The Meteoritical Society

Meteoritics & Planetary Science 55, Nr 5, 993–999 (2020)
doi: 10.1111/maps.13476

Sectioning effects of porphyritic chondrules: Implications for the PP/POP/PO classification and correcting modal abundances of mineralogically zoned chondrules

Jens BAROSCH*[1], Dominik C. HEZEL[1,2], Lena SAWATZKI[1], Lucia HALBAUER[1], and Yves MARROCCHI[3]

[1]Department of Geology and Mineralogy, University of Cologne, Zülpicher Str. 49b, 50674 Köln, Germany
[2]Department of Mineralogy, Natural History Museum, Cromwell Road, London SW7 5BD, UK
[3]CRPG, CNRS, Université de Lorraine, UMR 7358, Vandoeuvre-lès-Nancy 54501, France
*Corresponding author. E-mail: jbarosch@uni-koeln.de

(Received 16 April 2019; revision accepted 04 March 2020)

Abstract–Mineralogically zoned chondrules are a common chondrule type in chondrites. They consist of olivine cores, surrounded by low-Ca pyroxene rims. By serial sectioning porphyritic chondrules from carbonaceous, ordinary, and enstatite chondrites, we demonstrate that the 2-D textural appearances of these chondrules largely depend on where they are cut. The same chondrule may appear as a porphyritic pyroxene (PP) chondrule when sectioned through the low-Ca pyroxene rim, and as a porphyritic olivine-pyroxene (POP) or porphyritic olivine (PO) chondrule when sectioned close or through its equator. Chondrules previously classified into PP/POP/PO chondrules might therefore not represent different types, but various sections through mineralogically zoned chondrules. Classifying chondrule textures into PP, POP, and PO has therefore no unequivocal genetic meaning, it is merely descriptive. Sectioning effects further introduce a systematic bias when determining mineralogically zoned chondrule fractions from 2-D sections. We determined correction factors to estimate 3-D mineralogically zoned chondrule fractions when these have been determined in 2-D sections: 1.24 for carbonaceous chondrites, 1.29 for ordinary chondrites, and 1.62 for enstatite chondrites. Using these factors then shows that mineralogically zoned chondrules are the dominant chondrule type in chondrites with estimated 3-D fractions of 92% in CC, 52% in OC, and 46% in EC.

INTRODUCTION

Chondrules and fine-grained matrix are the two major components of chondrites. Chondrules are millimeter-sized igneous droplets mainly composed of silicates (olivine, pyroxene, plagioclase), Fe-Ni metal, sulfides, and a glassy or micro-crystalline mesostasis. A series of studies argued that chondrules formed in an open system and interacted with the ambient gas during their molten stage (Ebel et al. [2018] and references therein). Important support for this open system scenario is recorded in chondrules as a mineralogical and/or a compositional zonation (e.g., Tissandier et al. 2002; Hezel et al. 2003; Krot et al. 2004; Libourel et al. 2006; Nagahara et al. 2008; Friend et al. 2016; Marrocchi et al. 2018; Barosch et al. 2019; and references therein). The open system scenario constrains chondrule formation processes and explains various chondrule characteristics, such as the above-mentioned chondrule zonations or bulk compositional variations in chondrule populations.

Chondrules are classified either according to their textures and mineralogies, or their chemical compositions (cf. Scott and Krot [2014], and references therein). Three main classification schemes are commonly used. (i) Textural appearance—as introduced by Gooding and Keil (1981). The major textural categories are porphyritic olivine (PO), porphyritic pyroxene (PP), porphyritic olivine-pyroxene (POP), barred olivine (BO), and radial pyroxene (RP). Minor textural classifications, partly restricted to individual chondrite classes, are for example skeletal olivine (SO), granular olivine (GO), cryptocrystalline (C), or microporphyritic olivine chondrules (MPO). (ii) Bulk chondrule Si-concentration—these are the three types A (Si-

rich), AB (intermediate), and B (Si-poor). The distinction between Si-rich and -poor is only qualitative, not quantitative, and directly related to the textural types. PO are Si-poor, POP intermediate, and PP Si-rich. (iii) Chondrule olivine FeO-concentration—chondrules are divided into type I, when the chondrule olivine FeO content is below 10 wt%, and in type II, when the chondrule olivine FeO content is above 10 wt%. We note that various authors might, however, use different threshold values. Furthermore, this classification only works for unequilibrated samples with petrologic types below ~3.5. Another, though more rarely used, chemical chondrule classification is based on the cathodoluminescence activity of chondrule minerals (Sears et al. 1995). Lastly, a small number of chondrules are Al-rich with >10 wt% Al_2O_3 (Bischoff and Keil 1983).

Ideally, a chondrule classification provides genetic information. Chondrules are however mostly classified using 2-D sections, which are not necessarily representative of the 3-D chondrules (e.g., Hezel 2007; Ebel et al. 2009; Hezel and Kießwetter 2010; Cuzzi and Olson 2017; and references therein), and thus might skew any potential genetic information. If a sectioning bias is present in the majority of chondrules, the classification becomes meaningless or even incorrect. Mineralogically zoned chondrules might be particularly deceiving with regard to textural classification: they have an olivine core, surrounded by a low-Ca pyroxene rim, and their 2-D appearances depend on where they are sectioned. Classification of such mineralogically zoned chondrules in 2-D sections could therefore be unreliable, and might easily lead to misclassifications.

Here, we study this bias with sectioning experiments on chondrules in carbonaceous (CC; Efremovka CV3), ordinary (OC; Moorabie L3.8-an), and enstatite chondrite samples (EC; Sahara 97096 EH3, see Piani et al. 2012, 2016). In addition, we measured CM, CV, and CR chondrites (Table 1) with cabinet-sized microtomography to test whether this method can be used to study chondrule textures. The study of chondrules in 3-D allows" us to understand if, and to what extent their 2-D classification into PO/POP/PP, as well as A/AB/B depends on sectioning effects.

METHODS

Microtomography (μ-CT)

Micro-CT allows studying the petrography of a sample in 3-D (e.g., Ketcham 2005; Ebel et al. 2009; Beitz et al. 2013; Hezel et al. 2013; Hanna and Ketcham 2017), largely nondestructive (Sears et al. 2018) and noninvasive, and therefore seems to be the undisputed technique of choice for this study. This technique is nonetheless highly challenging for this kind of study, as μ-CT primarily images the density contrast between minerals. Olivine and pyroxene have very similar densities, with a span from 3.27 to 4.39 g cm^{-3} for forsterite and fayalite, and a span from 3.20 to 3.95 g cm^{-3} for enstatite and ferrosilite. We therefore performed a number of experiments with various measurement settings, as well as the two software packages ImageJ/Fiji and Avizo, to test whether the low-Ca pyroxene can be reliably discriminated from the olivine based on density contrasts.

Individual meteorite chips of a few mm in diameter were CT scanned in a Zeiss Xradia 520 Versa X-ray microscope at the Natural History Museum in London. Up to four chips were stacked upon each other in a plastic tube for a single experiment. Table 1 lists the settings used for the various experiments. The chips could only be a few mm in diameter to obtain the resolution of a few μm required to identify the often only tens of μm thick low-Ca pyroxene layers surrounding the olivine core. We therefore chose a chondrite group with many chondrules, but small chondrule sizes: CM, with average chondrules sizes of 145 μm (Friend et al. 2018); and two chondrite groups with large chondrule sizes, but then only few chondrules: CR and CV, with average chondrules sizes of 700 and 900 μm, respectively (Friedrich et al. 2015). All samples studied are listed in Table 1.

The resulting image stack was first processed with the Avizo software to correct for ring artifacts and reduce the noise as well as increase the contrast of the images using smoothing wave and enhancement filtering (cf. Li et al. 2017; Ni et al. 2017; Ferreira et al. 2018). As the olivine is slightly denser than the low-Ca pyroxene, olivine should appear slightly brighter than the pyroxene. Figure 1 displays a representative slice through Vigarano (CV3). It is almost impossible to unequivocally discriminate olivine from low-Ca pyroxene based on their respective different brightness. We also hoped to identify pyroxene by their characteristic 110 cleavages, which is principally very distinctive from the homogeneous appearance of olivine. However, the images were insufficiently resolved to unequivocally identify these cleavages.

In places where large pyroxenes or olivines could be identified, for example, based on their appearance with and without cleavages, we could measure the gray value changes across individual minerals. Such gray value difference across individual minerals was a few units, for example, two to five gray value units. However, absolute gray value differences between olivine and pyroxene were also in the range of about three to six gray value units. This means olivine and pyroxene gray values overlap already because of their individual gray value

Table 1. Measurement conditions for the various μ-CT experiments.

Samples*	Experiment	Current (μA)	Voltage (kV)	Exposure time (s)	Number of projections
Murchison (CM2)	1	80.2	50	2	3000
NWA801 (CR2)	2	80.2	50	5	6401
Vigarano (CV3)	3	80.2	30	20	6401
	4	75	40	5	6401
	5	80	40	5	6400
Cold Bokkeveld (CM2)	6	80	50	7	1601
	7	80	40	60	1601
Mokoia (CV3)	8	80	40	10	3201
Cold Bokkeveld (CM2)					
Jbilet Winselwan (CM2)					
Kaba (CV3)					

*The samples were stacked upon each other and all measured together in each experiment.

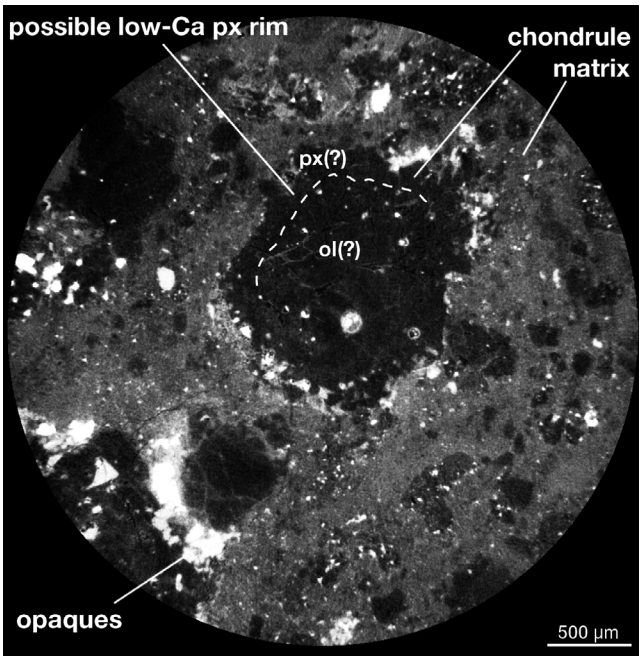

Fig. 1. A representative slice through the tomography image stack of Vigarano (CV3). The contact between olivine core and low-Ca pyroxene rim might be vaguely guessed, but cannot be determined reliably.

spread, resulting from mineral inhomogeneities. This makes it virtually impossible to threshold olivine from pyroxene using their gray values. This unfortunate result is true for all instrument settings we tested. And although in rare cases discriminating olivine from pyroxene may be possible, the density difference of olivine and low-Ca pyroxene in the samples studied and the instrument used was simply not enough for sufficiently reliable phase identification. Hence, reliably studying mineralogically zoned chondrules in 3-D with μ-CT based on phase density contrasts, and without crystallographic information, is not yet possible. We instead used 3-D serial sectioning for this study.

3-D Serial Sectioning

Serial sectioning, combined with scanning electron microscopy (SEM), allows 3-D reconstruction of chondrules. At first, a chondrite thick section was prepared by saw-cutting a large (0.5–1 cm-sized) chondrite chip, embedded in epoxy resin. The surface was polished with a diamond polishing compound. Then, the following three-step procedure was repeatedly carried out. (i) 2-D element maps of entire sample surfaces were recorded using an SEM (Zeiss Sigma 300 VP, located at the Institute of Geology and Mineralogy, Cologne). The focused electron beam rastered the stationary sample surface over small areas (~500 × 400 μm, pixel size ~4 μm). The aperture was set to 60 μm, the accelerating voltage to 20 kV, and the dwell time to 10 ms, resulting in a count rate of ~50,000 cps. The sample was then moved to a new position and the next map was obtained. All individual element maps were stitched together to a large area map (LAM), showing the entire chondrite section. (ii) From the LAM, a phase map was created using the PHAPS program (Hezel 2010). Every color in the phase map represents a different mineral phase, allowing instant visual identification of chondrule textures. (iii) Finally, the sample was ground down a few tens of μm and again polished with a diamond polishing compound.

Each large-area phase map represents a different section perpendicular to the *z*-axis of the sample and, when stacked on top of each other, the resulting image stack allows 3-D insights into the sample. The amount of grounding in each step was monitored using a slide gauge. In addition, two precise aluminum cones were embedded on opposing sides of every sample thick section. The basal cone diameters were measured at each sectioning step and the difference to the previous section was used to calculate the slice of material removed by grinding. Depending on the sample, typical

abrasion thicknesses varied between 20 and 120 μm. In Efremovka and Moorabie, on average, ~80 μm was ground down in each step. Grinding step sizes were smaller for Sahara 97096, with on average ~40 μm. This was done for ~10 sections for each of the three chondrites. We then obtained 3-D chondrule images by tracing the chondrules through the phase maps of the neighboring sections.

RESULTS

Sectioning Effects When Classifying Chondrules

Three unequilibrated chondrites were serial sectioned—covering all three chondrite classes—and their chondrules studied in 2-D and 3-D: Efremovka (CV3; 86 chondrules), Moorabie (L3.8-an; 117 chondrules), and Sahara 97096 (EH3; 252 chondrules). Mineralogically zoned chondrules typically consist of an olivine core surrounded by a low-Ca pyroxene rim of variable thickness (cf. examples in Fig. 2). We designate chondrules based on their mineral modal abundances as follows: PP (with ol/px $\leq$0.1), POP, and PO (with ol/px $\geq$0.9).

The apparent 2-D textural appearances of mineralogically zoned chondrules vary, depending on where a chondrule is sectioned (Fig. 2). A 2-D section close to the chondrule border will cut through the low-Ca pyroxene rim, and the chondrule texture appears as PP. Small olivine grains are often poikilitically enclosed in the rim pyroxene crystals, but in some rims, olivine is completely absent. In sections closer to the equator of a chondrule, the olivine plus mesostasis-rich core is cut, and the apparent 2-D texture is POP, due to the commonly still high abundance of pyroxene. A section close or through the chondrule equator is the most likely to appear as a PO texture, depending on the thickness of the pyroxene rim. We found only three Efremovka (CV) chondrules that had PP textures in every section through these chondrules. PP chondrules were naturally more common in the enstatite chondrite Sahara 97096, with a 3-D fraction of ~60%.

Examples for the sectioning effects are displayed in Fig. 2: Row a—the Efremovka chondrule rim section has an apparent PP 2-D texture but then shows an apparent POP texture in sections located in-between border and equator, and finally an apparent PO texture when sectioned directly through its equator. This example also demonstrates how the mineralogical zonation of this chondrule is disguised in the rim section by the apparent PP texture. We further note that the apparent chondrule diameter increases from PP (smallest diameter) to POP (intermediate) and lastly, to PO (largest). Row b—the Moorabie chondrule has an apparent PP 2-D texture in the section through its rim, again disguising the zoned nature of this chondrule. The sections closer to and directly through this chondrule's equator then result in apparent POP textures. Row c—enstatite chondrite chondrules almost always appear as PP chondrules due to their thick low-Ca pyroxene rims. Tiny olivine cores are, however, highly abundant in EC chondrules (see also Piani et al. 2016). The example demonstrating this in Fig. 2 is a chondrule from Sahara 97096.

Sectioning Effects When Determining the Fraction of Mineralogically Zoned Chondrules

To determine 2-D and 3-D zoned chondrule fractions in all three samples, we first picked the middle sections of each sample's image stack for 2-D evaluations. Every chondrule studied in 2-D in these sections was subsequently studied in 3-D, by tracing it through the phase maps of the neighboring sections. The zoned chondrule fractions determined from 2-D sections are 64% in Efremovka (86 chondrules studied in total), 42% in Moorabie (117 chondrules studied in total), and 26% in Sahara 97096 (252 chondrules studied in total). The zoned chondrule fractions of the same chondrules, but determined in 3-D, are significantly and systematically higher: 79% in Efremovka, 54% in Moorabie, and 43% in Sahara 97096. In relative proportions, the increase from 2-D to 3-D zoned chondrule fractions are +24% (i.e., by factor 1.24) in Efremovka, +29% (i.e., by factor 1.29) in Moorabie, and +62% (i.e., by factor 1.62) in Sahara 97096 (Fig. 3).

DISCUSSION AND SUMMARY

A classification scheme for chondrule textures can ideally be used to draw conclusions about their formation processes. It is therefore critical that such a scheme does not provide misleading information. Chondrule textures are first discriminated into porphyritic and non-porphyritic chondrules. Different thermal histories apply to these types: porphyritic chondrules crystallized from melts with abundant nuclei after incomplete melting of precursor materials (Lofgren 1996; Connolly et al. 1998; Marrocchi et al. 2018, 2019), while non-porphyritic chondrules likely crystallized from superheated melts without nuclei (e.g., Connolly and Hewins 1995). Porphyritic chondrules are then classified into PP, PO, and POP (e.g., Gooding and Keil 1981). This classification is, however, not always meaningful and can be misleading, as most chondrules are studied in 2-D only. We demonstrate in Fig. 2 that an individual porphyritic zoned chondrule can be classified

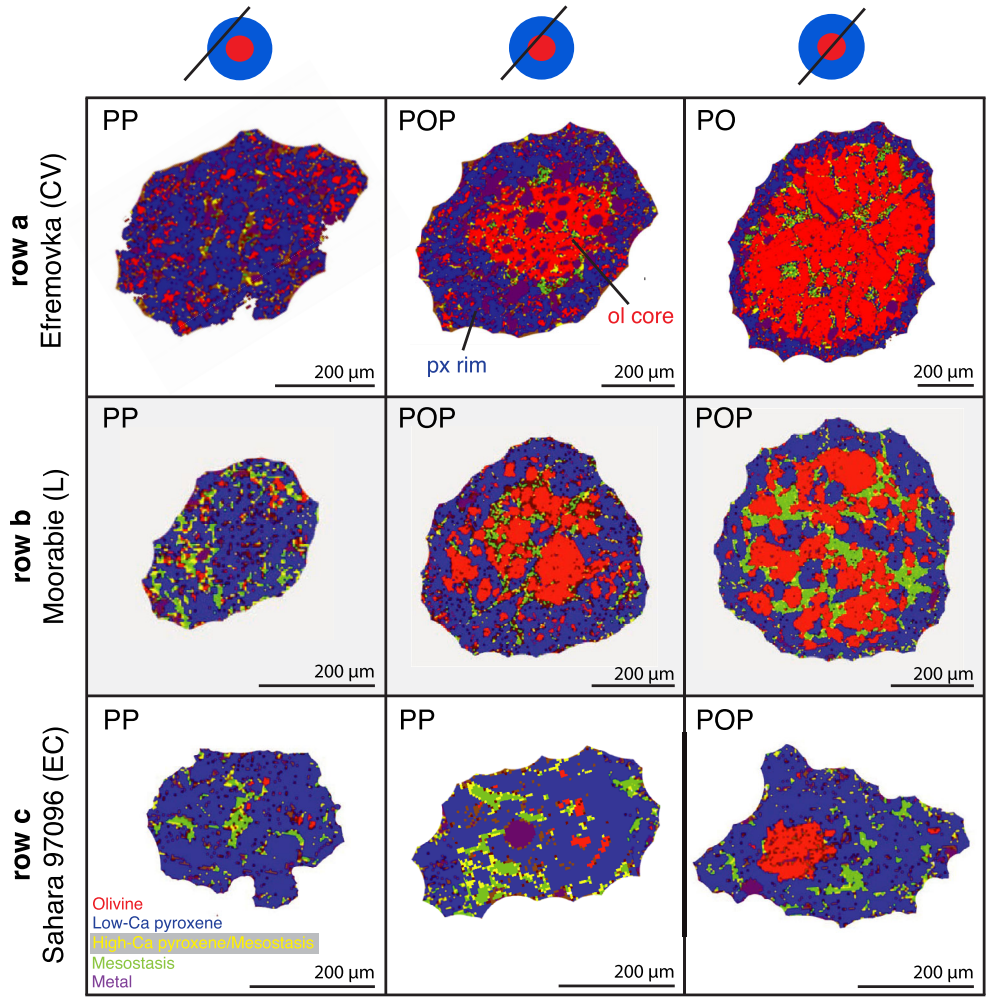

Fig. 2. Different sections through single chondrules in Efremovka, Moorabie, and Sahara 97096 are displayed. The apparent 2-D textures and, hence, their classifications into PP, PO, or POP, depend on where a chondrule is sectioned. Chondrule diameters in row a, and b, apparently increase from PP (smallest) to POP (intermediate) to PO (largest diameter). (Color figure can be viewed at wileyonlinelibrary.com.)

as PP, POP, and PO, solely based on where it was sectioned. Thus, discriminating between PP, POP, and PO chondrules often only indicates where a chondrule was cut, but does not necessarily reveal useful genetic information. This then also applies to the subclassification of chondrules into A (Si-rich), AB (intermediate), and B (Si-poor), as this is directly related to the textural types PP, POP, and PO. Therefore, the same argument applies to this classification scheme: It is largely controlled by sectioning effects. However, not all 2-D PP chondrules are rim sections: we indeed find entire PP chondrules in 3-D. These are very common in the EC sample, rare in the OC sample, and very rare in the CC sample. Using a subset of our data, we estimate the true (3-D) fraction of PP chondrules to ~60% in the EC sample and to ~7% in the CC sample. This is significantly lower than the 2-D PP chondrule fractions of ~80% in EC and 30% in CC, thereby further illustrating the sectioning problem. Hence, in CC, where most chondrules are mineralogically zoned, the vast majority of PP chondrules—as observed in 2-D sections—are actually rim sections of POP/PO chondrules.

Based on the aforementioned observations, it is clear that the textural classification of porphyritic chondrules needs to be used with caution. Designating chondrules as either mineralogically zoned (MZ) chondrules or mineralogically unzoned (MU) chondrules might be a useful addition to the PP, POP, PO classification, as it adds currently missing textural information. However, reliably identifying zoned chondrules in 2-D sections is as well problematic. Therefore, deciding which classification scheme is used might depend on what specific problem is studied. All we need to do here is to clearly point out and quantify the sectioning effects with regard to

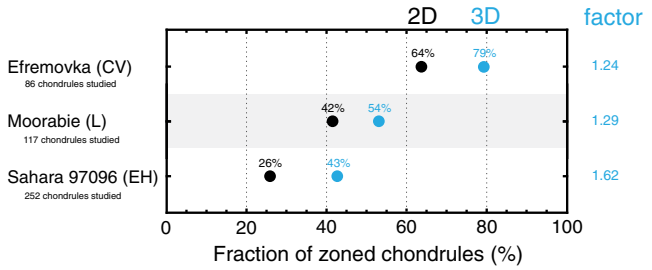

Fig. 3. Here, 2-D and 3-D zoned chondrule fractions have been determined in the same samples. The fraction of zoned chondrules is always higher when determined in 3-D, demonstrating the systematic bias when the fraction of zoned chondrules is determined in 2-D. These 2-D–3-D differences can be used as approximate correction factors to estimate the true 3-D fraction of zoned chondrules from a determined 2-D fraction. (Color figure can be viewed at wileyonlinelibrary.com.)

mineralogically zoned chondrules. This is of great importance, as these are—as demonstrated below—the dominant chondrule type in most chondrites.

Mineralogically zoned chondrules sectioned through their low-Ca pyroxene rims usually appear as unzoned. Consequently, the fractions of mineralogically zoned chondrules in chondrites are underestimated in 2-D studies (e.g., Friend et al. 2016; Barosch et al. 2019). Determining true zoned chondrule fractions requires 3-D textural analysis, for example, serial sectioning. With this technique, we studied chondrules in 3-D, excluding all sectioning effects. We determined the following correction factors for estimating true 3-D fractions from measured 2-D fractions: 1.24 for CC, 1.29 for OC, and 1.62 for EC (Fig. 3).

The weighted average 2-D zoned chondrule fractions reported in previous studies, and including the new 2-D data reported in this study, are ~74% in CC (Friend et al. 2016), ~40% in OC (Barosch et al. 2019), and ~29% in EC (unpublished). The 3-D corrected, i.e., estimated true average zoned chondrule fractions are then: 92% in CC, 52% in OC, and 46% in EC. This makes mineralogically zoned chondrules the dominant chondrule type in chondrites.

Acknowledgments—We thank Hanna Cieszynski for her assistance operating the SEM and Kathrin Jung for sample preparation. DH is grateful for a Europlanet grant to the London Natural History Museum that was essential for this study. Europlanet 2020 RI has received funding from the European Union's Horizon 2020 research and innovation program under grant agreement No. 654208. This study was funded by the Deutsche Forschungsgemeinschaft (DFG) grants HE 5352/10-1 and PA 346/50-1. We thank G. Libourel and A. N. Krot for their thorough and helpful reviews, as well as associate editor K. Righter for handling the manuscript.

Editorial Handling—Dr. Kevin Righter

REFERENCES

Barosch J., Hezel D. C., Ebel D. S., and Friend P. 2019. Mineralogically zoned chondrules in ordinary chondrites as evidence for chondrule open system behaviour. *Geochimica et Cosmochimica Acta* 249:1–16.

Beitz E., Blum J., Mathieu R., Pack A., and Hezel D. C. 2013. Experimental investigation of the nebular formation of chondrule rims and the formation of chondrite parent bodies. *Geochimica et Cosmochimica Acta* 116:41–51.

Bischoff A. and Keil K. 1983. Al-rich objects in ordinary chondrites: related origin of carbonaceous and ordinary chondrites and their constituents. *Geochimica et Cosmochimica Acta* 48:693–709.

Connolly Jr. H. C. and Hewins R. 1995. Chondrules as products of dust collisions with totally molten droplets within a dust-rich nebular environment: An experimental investigation. *Geochimica et Cosmochimica Acta* 59:3231–3246.

Connolly Jr. H. C., Jones B. D., and Hewins R. H. 1998. The flash melting of chondrules: An experimental investigation into the melting history and physical nature of chondrule precursors. *Geochimica et Cosmochimica Acta* 62:2725–2735.

Cuzzi J. N. and Olson D. M. 2017. Recovering 3D particle size distributions from 2D sections. *Meteoritics & Planetary Science* 52:532–545.

Ebel D. S., Leftwich K., Brunner C. E., and Weisberg M. K. 2009. Abundance and size distribution of inclusions in CV3 chondrites by X-ray image analysis (abstract #2065). 40th Lunar and Planetary Science Conference. CD-ROM.

Ebel D. S., Alexander C. M.O'D., and Libourel G. 2018 Vapor-melt exchange. In *Chondrules: Records of protoplanetary disk processes*, edited by Russell S. S., Connolly Jr. H. C. and Krot A. N. Cambridge, UK: Cambridge University Press. pp. 151–174.

Ferreira T. R., Pires L. F., Wildenschild D., Heck R. J., and Antonino A. C. 2018. X-ray microtomography analysis of lime application effects on soil porous system. *Geoderma* 324:119–130.

Friedrich J. M., Weisberg M. K., Ebel D. S., Biltz A. E., Corbett B. M., Iotzov I. V., Khan W. S., and Wolman M. D. 2015. Chondrule size and related physical properties: A compilation and evaluation of current data across all meteorite groups. *Geochemistry* 75:419–443.

Friend P., Hezel D. C., and Mucerschi D. 2016. The conditions of chondrule formation, Part II: Open system. *Geochimica et Cosmochimica Acta* 173:198–209.

Friend P., Hezel D. C., Barrat J. A., Zipfel J., Palme H., and Metzler K. 2018. Composition, petrology and chondrule-matrix complementarity of the recently discovered Jbilet Winselwan CM2 chondrite. *Meteoritics & Planetary Science* 53:2470–2491.

Gooding J. L. and Keil K. 1981. Relative abundances of chondrule primary textural types in ordinary chondrites and their bearing on conditions of chondrule formation. *Meteoritics* 16:17–43.

Hanna R. D. and Ketcham R. A. 2017. X-ray computed tomography of planetary materials: A primer and review of recent studies. *Geochemistry* 77:547–572.

Hezel D. C. 2007. A model for calculating the errors of 2D bulk analysis relative to the true 3D bulk composition of an object, with application to chondrules. *Computers & Geosciences* 33:1162–1175.

Hezel D. C. 2010. A Mathematica code to produce phase maps from two element maps. *Computers & Geosciences* 36:1097–1099.

Hezel D. C. and Kießwetter R. 2010. Quantifying the error of 2D bulk chondrule analyses using a computer model to simulate chondrules (SIMCHON). *Meteoritics & Planetary Science* 45:555–571.

Hezel D. C., Palme H., Brenker F. E., and Nasdala L. 2003. Evidence for fractional condensation and reprocessing at high temperatures in CH-chondrites. *Meteoritics & Planetary Science* 38:1199–1216.

Hezel D. C., Elangovan P., Viehmann S., Howard L., Abel R. L., and Armstrong R. 2013. Visualisation and quantification of CV chondrite petrography using micro-tomography. *Geochimica et Cosmochimica Acta* 116:33–40.

Ketcham R. A. 2005. Computational methods for quantitative analysis of three-dimensional features in geological specimens. *Geosphere* 1:32–41.

Krot A. N., Libourel G., Goodrich C. A., and Petaev M. I. 2004. Silica-rich igneous rims around magnesian chondrules in CR carbonaceous chondrites: Evidence for condensation origin from fractionated nebular gas. *Meteoritics & Planetary Science* 39:1931–1955.

Li Z., Liu D., Cai Y., Ranjith P. G., and Yao Y. 2017. Multi-scale quantitative characterization of 3-D pore-fracture networks in bituminous and anthracite coals using FIB-SEM tomography and X-ray μ-CT. *Fuel* 209:43–53.

Libourel G., Krot A. N., and Tissandier L. 2006. Role of gas–melt interaction during chondrule formation. *Earth and Planetary Science Letters* 251:232–240.

Lofgren G. 1996. A dynamic crystallization model for chondrules melts. In *Chondrules and the protoplanetary disk*, edited by Hewins R. H., Jones R. H., and Scott E. R. D. Cambridge, UK: Cambridge University Press. pp. 1887–1896.

Marrocchi Y., Villeneuve J., Batanova V., Piani L., and Jacquet E. 2018. Oxygen isotopic diversity of chondrule precursors and the nebular origin of chondrules. *Earth and Planetary Science Letters* 496:132–141.

Marrocchi Y., Euverte R., Villeneuve J., Batanova V., Welsch B., Ferrière L., and Jacquet E. 2019. Formation of CV chondrules by recycling of amoeboid olivine aggregate-like precursors. *Geochimica et Cosmochimica Acta* 247:121–141.

Nagahara H., Kita N. T., Ozawa K., and Morishita Y. 2008. Condensation of major elements during chondrule formation and its implication to the origin of chondrules. *Geochimica et Cosmochimica Acta* 72:1442–1465.

Ni X., Miao J., Lv R., and Lin X. 2017. Quantitative 3D spatial characterization and flow simulation of coal macropores based on μCT technology. *Fuel* 200:199–207.

Piani L., Robert F., Beyssac O., Binet L., Bourot-Denise M., Derenne S., Le Guillou C., Marrocchi Y., Mostefaoui S., Rouzaud J.-N., and Thomen A. 2012. Structure, composition and location of the organic matter found in the enstatite chondrite Sahara 97096 (EH3). *Meteoritics & Planetary Science* 47:8–29.

Piani L., Marrocchi Y., Libourel G., and Tissandier L. 2016. Magmatic sulfides in the porphyritic chondrules of EH enstatite chondrites. *Geochimica et Cosmochimica Acta* 195:84–99.

Scott E. R. D., and Krot A. N. 2014. Chondrites and their components. In *Treatise on geochemistry*, 2nd ed., edited by Holland H. and Turekian K. Oxford: Elsevier. pp. 65–137.

Sears D. W. G., Morse A. D., Hutchison R., Guimon R. K., Jie L., Alexander C. M. O'D, Benoit P. H., Wright I., Pillinger C., Xie T., and Lipschutz M. E. 1995. Metamorphism and aqueous alteration in low petrographic type ordinary chondrites. *Meteoritics* 30:169–181.

Sears D. W. G., Sehlke A., Friedrich J. M., Rivers M. L., and Ebel D. S. 2018. X-ray computed tomography of extraterrestrial rocks eradicates their natural radiation record and the information it contains. *Meteoritics & Planetary Science* 53:2624–2631.

Tissandier L., Libourel G., and Robert F. 2002. Gas-melt interactions and their bearing on chondrule formation. *Meteoritics & Planetary Science* 37:1377–1389.